

Analysis of optical characteristics of modulation devices with square and circle pixels for 3D holographic display

Xiao Ma (马晓), Juan Liu (刘娟)*, Zhao Zhang (张昭), Xin Li (李昕),
Jia Jia (贾甲), Bin Hu (胡滨), and Yongtian Wang (王涌天)

Beijing Engineering Research Center for Mixed Reality and Novel Display Technology,
Key Laboratory of Photo Electronic Imaging Technology and System, Ministry of
Education of China, School of Optics and Electronics, Beijing Institute of Technology,
Beijing 100081, China

*Corresponding author: juanliu@bit.edu.cn

Received August 3, 2014; accepted October 24, 2014; posted online December 30, 2014

With the development of the micro/nanolithography, the optic-optic or optic-electronic modulation devices with different pixel shapes and sizes can be used for three-dimensional (3D) dynamical holographic display. The influence of different parameters of the modulation devices on the image quality of the 3D reconstructed object is analyzed for two cases: the phase-only computer-generated holography (CGH) and the complex amplitude CGH. The results quantitatively show that the pixel shape of the modulation devices will affect the quality of the holographic image.

OCIS codes: 090.2870, 090.1760, 090.1995.
doi: 10.3788/COL201513.010901.

Holography is an ideal three-dimensional (3D) display technique because it can reconstruct the wavefront of the actual 3D objects^[1,2]. Computer-generated holography (CGH) can produce accurate depth cues of 3D objects existing or never existing in the real world^[3,4]. Because of the flexibility in controlling wavefronts, spatial light modulators (SLMs), whether optic-optic modulation devices or optoelectronic modulation devices, have been widely suggested for realizing 3D dynamic holographic display^[5,6], and their parameters will greatly affect the image quality.

The field of view (FOV) and the reconstructed size of the 3D image are important parameters in 3D holographic display. The size and the viewing zone of the reconstructed 3D optical image are limited by space-bandwidth product of the SLMs^[7-11]. As is known, higher resolution and smaller pixel pitch of the SLMs allow larger viewing zone and bigger image size. The zero-order spot caused by the dead space areas of the pixelated SLMs^[12] is a serious problem in 3D holographic display and has drawn some attention^[12-16] in recent years. Different pixel shapes and sizes of the pixelated SLM will influence the image quality, the FOV, and the image size. Recently, the femtosecond pulse technology used for 3D holographic display was reported^[17], and this technology can produce optic-optic modulation devices with circle pixel. However, to the best of our knowledge, the SLM with circle pixel has not yet been investigated. In this letter, we investigate their optical characteristics and make a comprehensive analysis of the effect of the pixel's shape on the reconstructed 3D image quality.

The diagram of holographic reconstruction process is shown in Fig. 1. β_{\max} is the maximum diffraction angle, H is the width of the CGH (it will load on the SLM), D is the maximum size of the reconstructed image, l is the reconstructed distance, θ is the maximum viewing angle, and b is the view distance. Now we consider different pixel shapes: the square and the circle pixels, of the SLM, respectively.

According to the diffraction theory, when the pixel shape is square, the diffraction angle β_{\max} is calculated as^[18]

$$\beta_{\max} = \tan^{-1} \left(\frac{\lambda}{p} \right), \quad (1)$$

where p is the pixel pitch, λ is the wavelength in free space. According to the triangular geometry relationship, one can calculate the diffraction angle as

$$\beta_{\max} = \tan^{-1} \left(\frac{H/2 + D/2}{l} \right), \quad (2)$$

and the maximum size of the reconstructed image D as

$$D = \frac{2\lambda l}{p} - H. \quad (3)$$

The size of the reconstructed image is inversely proportional to the pixel pitch, and the smaller pixel pitch will cause the larger reconstructed image.

The FOV can be written as

$$\theta = 2 \tan^{-1} \left(\frac{|H - \lambda l/p|}{l} \right). \quad (4)$$

It is restricted by the pixel pitch and the size of the CGH when the reconstructed distance l and wavelength λ are fixed.

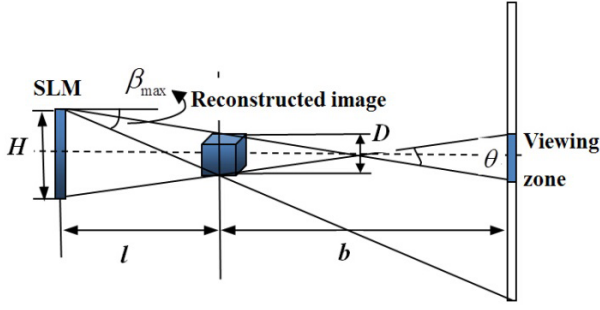


Fig. 1. Diagram of holographic reconstruction process.

When the pixel shape of the SLM is circle, the complex amplitude transmission of the pixelated SLM can be expressed as

$$t(x, y) = \left[\text{circ} \left(\frac{\sqrt{x^2 + y^2}}{r} \right) \otimes \frac{1}{d_x d_y} \text{comb} \left(\frac{x}{d_x}, \frac{y}{d_y} \right) \right] \cdot \text{rect} \left(\frac{x}{l_x}, \frac{y}{l_y} \right), \quad (5)$$

where r denotes the radius of the pixel, $d_i (i = x, y)$ and $l_i (i = x, y)$ denote the pixel pitch and the size of the SLM. The Fourier transform of $t(x, y)$ can be expressed as

$$T(f_x, f_y) = \left[\pi r^2 \frac{J_1 \left(2\pi r \sqrt{f_x^2 + f_y^2} \right)}{2\pi r \sqrt{f_x^2 + f_y^2}} \cdot d_x d_y \text{comb}(f_x d_x, f_y d_y) \right] \otimes l_x l_y \text{sinc}(f_x l_x, f_y l_y). \quad (6)$$

The useful diffraction order is in the center of the spectrogram and the range of the diffraction angle is determined by the first-order Bessel function. According to the diffraction limitation, the diffraction angle can be expressed as

$$\beta'_{\max} = \tan^{-1} \left(\frac{1.22\lambda}{p} \right). \quad (7)$$

Compared with the square pixel case, the maximum size of the reconstructed image and viewing angle are weighted with the parameter 1.22. So the formulae of the maximum size of the reconstructed image and viewing angle can be expressed as

$$D' = \frac{2 \times 1.22\lambda l}{p} - H, \quad (8)$$

$$\theta' = 2 \tan^{-1} \left(\frac{|H - 1.22\lambda l/p|}{l} \right). \quad (9)$$

A commercial SLM is pixelated and when it is employed for holographic projection of arbitrary light patterns, the zero-order beam exists in the image plane. We then consider the zero-order spot of the SLMs with different pixel shapes.

For the square pixel shape of the SLM, the light distribution in the center of the reconstruction plane can be described as^[16]

$$T(0, 0) = \mu E(0, 0) + (1 - \mu)F(0, 0), \quad (10)$$

where μ is the fill factor of the square pixel shape SLM, and^[16]

$$E(f_x, f_y) = \mathfrak{F}\{\exp[i\phi_{\text{ac}}(x, y)]\}, \quad (11)$$

$$F(f_x, f_y) = \mathfrak{F}\{A_{\text{ds}}(x, y) \exp[i\phi_{\text{ds}}(x, y)]\}, \quad (12)$$

where E and F are the Fourier transforms of the active areas distribution and dead space areas distribution. x and y denote the spatial frequencies in the image plane, and f_x and f_y denote the spatial frequencies in the reconstructed plane. $\phi_{\text{ac}}(x, y)$ is the active areas distribution, $A_{\text{ds}}(x, y)$ and $\phi_{\text{ds}}(x, y)$ denote the amplitude and the phase modulations of the dead space areas.

For the circle pixel shape of the SLM, the transmittance of the dead space areas can be written as

$$t'_{\text{ds}}(x, y) = \left\{ \text{rect} \left(\frac{x}{d_x}, \frac{y}{d_y} \right) - \text{circ} \left(\frac{\sqrt{x^2 + y^2}}{a} \right) \right\} \otimes \frac{1}{d_x d_y} \text{comb} \left(\frac{x}{d_x}, \frac{y}{d_y} \right) \cdot A'_{\text{ds}}(x, y) \cdot \exp[i\phi'_{\text{ds}}(x, y)], \quad (13)$$

where a and $d_i (i = x, y)$ denote the radius of the pixel and the period, respectively, $A'_{\text{ds}}(x, y)$ and $\phi'_{\text{ds}}(x, y)$ denote the amplitude and the phase modulations of the dead space areas.

The complex amplitude distribution in the reconstruction plane can be calculated as the Fourier transform of $t'_{\text{ds}}(x, y)$, that is, $T'_{\text{ds}}(f_x, f_y)$, which can be expressed as

$$T'_{\text{ds}}(f_x, f_y) = \left[\left\{ d_x d_y \text{sinc}(f_x d_x, f_y d_y) - \pi a^2 \frac{J_1 \left(2\pi a \sqrt{f_x^2 + f_y^2} \right)}{2\pi a \sqrt{f_x^2 + f_y^2}} \right\} \otimes F'(f_x, f_y) \right], \quad (14)$$

where F' is the Fourier transform of the dead space areas distribution

$$F'(f_x, f_y) = \mathfrak{F}\{A'_{\text{ds}}(x, y) \exp[i\phi'_{\text{ds}}(x, y)]\}. \quad (15)$$

It is easy to demonstrate that when $\sqrt{f_x^2 + f_y^2}$ is equal

to 0, the expression $\frac{J_1 \left(2\pi a \sqrt{f_x^2 + f_y^2} \right)}{2\pi a \sqrt{f_x^2 + f_y^2}}$ in Eq. (14) is

equal to 1^[19]. So the result of $T'_{\text{ds}}(0, 0)$ can be calculated as

$$T'_{\text{ds}}(0, 0) = (d_x d_y - \pi a^2)F(0, 0). \quad (16)$$

The light distribution in the center of the reconstruction plane can be described as

$$T'(0, 0) = \frac{\pi a^2}{d_x d_y} E'(0, 0) + \frac{1 - \pi a^2}{d_x d_y} F'(0, 0) = \mu' E'(0, 0) + (1 - \mu') F'(0, 0), \quad (17)$$

where μ' is the fill factor of the circle pixel shape SLM, and

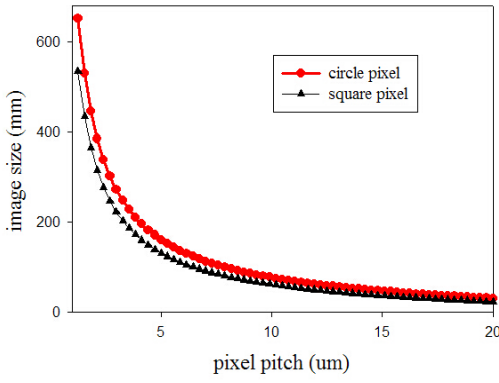


Fig. 2. Variation of reconstruction image size with pixel pitch for the square and circle pixel shape cases.

$$E'(f_x, f_y) = \mathfrak{F}\{\exp[i\phi_{ac}'(x, y)]\}. \quad (18)$$

It is obvious that the zero-order spot will be influenced by the fill factor of SLM and the amplitude modulation of dead space area. The zero-order spots are the same both for the modulation devices with the circle and the square pixel shapes.

We use peak signal-to-noise ratio (PSNR) and the diffraction efficiency to evaluate the quality of the reconstructed image. The definition of PSNR is^[19]

$$\text{PSNR} = 10 \times \log_{10} \left(\frac{(2^n - 1)^2}{\text{MSE}} \right), \quad (19)$$

where n is the bit depth of the image, and

$$\text{MSE} = \frac{1}{MN} \sum_{n=1}^N \sum_{m=1}^M \|I(m, n) - K(m, n)\|^2, \quad (20)$$

where $M \times N$ is the image's resolution, and I, K indicate the reconstructed image and the original image. Generally, a higher PSNR indicates that the reconstructed image is with higher quality.

To compare the relationship of the pixel pitch with image size for the cases of square and circle pixels, we now perform numerical simulations.

The parameters used in the simulations are as follows: the illuminating wavelength is 632.8 nm, the resolution of the SLM is 512×512, and the reconstructed distance is 500 mm. All the other parameters are kept unchanged except that the pixel pitch is varied from 1 to 20 μm . When the pixel pitch is smaller than the wavelength, the Fourier optics theory is not valid. The results are shown in Fig. 2. It can be seen that the image size is decaying rapidly with the increase in the pixel pitch when it is less than 5 μm and the size is a bit larger in the circle pixel case.

To compare the relationship of the pixel pitch with the viewing angle for the cases of square and circle pixels, we now perform the numerical simulations.

All the parameters are kept unchanged except that the pixel pitch is changed from 1 to 20 μm . The results are shown in Fig. 3. One can find that the viewing angle increases as the pixel pitch decreases, and when the pixel pitch is less than 5 μm , the viewing angle

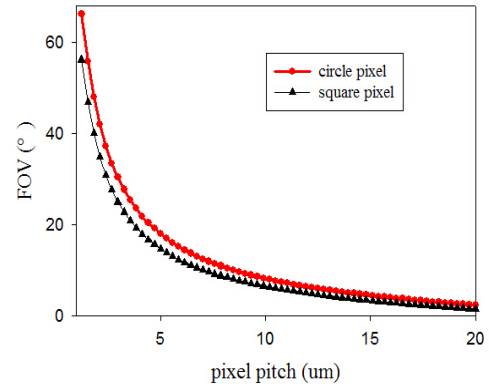


Fig. 3. Variation of FOV with pixel pitch for the square and circle pixel shape cases.

increases rapidly. In the circle pixel case, the viewing angle is a little bigger than the square pixel case.

To investigate the effect of the limited fill factor on the quality of the reconstructed image, we consider the numerical simulation for both the square and circle pixels. The complex amplitude CGH and phase-only CGH cases are both carried out.

Firstly, the complex amplitude modulated CGH is simulated. We use two images with the propagation distances 300 and 600 mm to simulate the 3D scene. The results shown in the letter are obtained with the parameters as: a 20×20 matrix is used to denote one pixel of SLM and the resolution of the original image and the SLM is 64×64. The angular spectrum method is used to calculate the propagation process. In order to facilitate the calculation, the fill factor is changed from 0% to 90.25% for the square pixel case, and from 0% to 78.53% for the circle pixel case. The results are shown in Fig. 4. Figure 5 shows the reconstructed images that are focused on the image “dog” (300 mm) for different fill factors and pixel shapes. Figure 4 shows that the reconstructed image quality by the circle pixel shape of the SLM is higher than that of the square pixel case. It is found that the energy efficiencies are almost the same for both the circle and

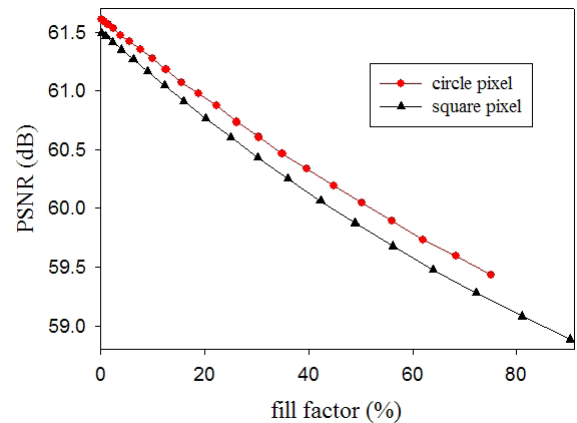


Fig. 4. Variation of PSNR with the fill factor for the square and circle pixel shape cases when the CGH is complex amplitude.



Fig. 5. Reconstructed images focused on “dog” for different fill factors and pixel shapes: fill factor of (a) 81% and (b) 12.25% for square pixel shape; (c) 78.53% and (d) 12.56% for circle pixel shape.

the square pixel cases. The results in Fig. 5 show that with the smaller fill factor, the reconstructed image is clearer.

Then the phase-only CGH is considered for the square and the circle pixel cases, respectively. All the parameters remain unchanged. The results are shown in Fig. 6. Because the actual SLM is more than 60% of the fill factor, the circle pixel case can reach higher image quality in the actual applications. The energy efficiencies almost have no difference for both the circle and square pixel cases.

To compare the influence of the amplitude modulation of the dead space on the intensity of zero-order beam, we simulate both cases: square and circle pixel shapes of the SLM.

The complex amplitude CGH and phase-only CGH are simulated. The amplitude changes from 0 to 1. To compare different pixel shapes, we choose two approximately equal fill factors: 49% for square pixel case and 50.3% for the circle case. The results are shown in Fig. 7 when the CGH is complex amplitude and in Fig. 8 when CGH is phase-only. It is shown that the relationship of the zero-order’s intensity with the amplitude of dead area is almost the same for both

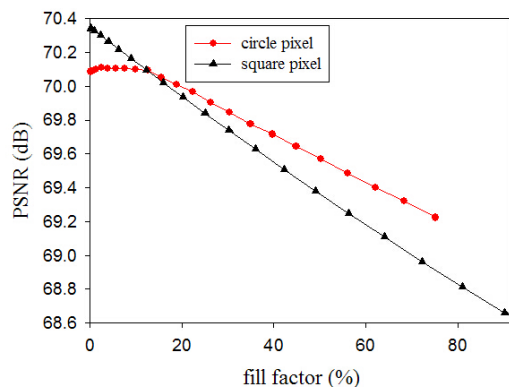


Fig. 6. Variation of PSNR with the fill factor for the square and circle pixel shape cases when the CGH is phase-only.

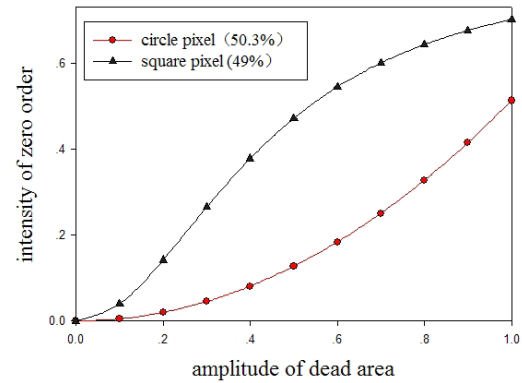


Fig. 7. Variation of intensity of zero-order spot with the amplitude of dead area for the square and circle pixel shape cases when the CGH is complex amplitude.

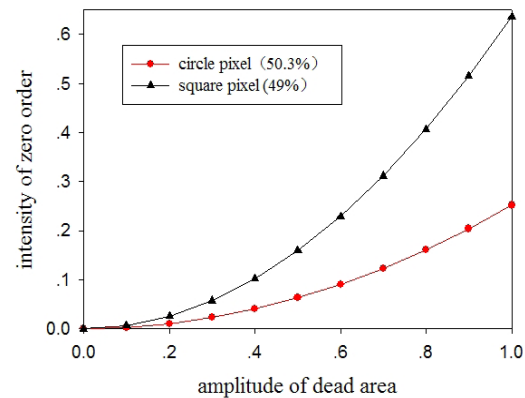


Fig. 8. Variation of intensity of zero-order spot with the amplitude of dead area for the square and circle pixel shape cases when the CGH is phase-only.

the complex amplitude and the phase-only cases. One can find that both in the square and circle pixel cases, the intensity of zero order increases as the amplitude modulation increases. When the fill factors are nearly equal, zero-order spot intensity from the circle pixel is lower than that of the square case, which means the efficiency is higher for the circle pixel case.

In conclusion, we quantitatively analyze the influence of different parameters of SLM on the reconstructed image quality for the cases of square and circle pixels. The circle pixel case will lead to slightly bigger reconstructed image, slightly larger viewing angle, better image quality, and higher space frequency of the reconstructed image. Smaller fill factor of SLM can improve the quality of the image when the pixel pitch is fixed. This investigation will provide useful information for realizing 3D holographic display in the future.

This work was supported by the National 973 Program of China (Nos. 2013CB328801 and 2013CB328806) and the National Natural Science Foundation of China (No. 61235002).

References

1. M. Sha, J. Liu, X. Li, and Y. Wang, *Chin. Opt. Lett.* **12**, 060023 (2014).
2. H. Yoshikawa and T. Yamaguchi, *Chin. Opt. Lett.* **9**, 120006 (2011).
3. A. Stein, Z. Wang, and J. J. S. Leigh, *Comput. Phys.* **6**, 389 (1992).
4. C. Slinger, C. Cameron, and M. Stanley, *Computer* **38**, 46 (2005).
5. N. Matsumoto, T. Inoue, and H. Toyoda, *Opt. Lett.* **37**, 3135 (2012).
6. S. Zwick, T. Haist, M. Warber, and W. Osten, *Appl. Opt.* **49**, F47 (2010).
7. N. Fukaya, K. Maeno, O. Nishikawa, K. Matumoto, K. Sato, and T. Honda, *Proc. SPIE* **2406**, 283 (1995).
8. T. Kozacki, M. Kujawińska, G. Finke, B. Hennelly, and N. Pandey, *Appl. Opt.* **51**, 1771 (2012).
9. J. Jia, Y. Wang, J. Liu, X. Li, and J. Xie, *Opt. Eng.* **50**, 115801 (2011).
10. Y. Takaki and Y. Hayashi, *Appl. Opt.* **47**, D6 (2008).
11. Y. Z. Liu, X. N. Pang, S. Jiang, and J. W. Dong, *Opt. Express* **21**, 12069 (2013).
12. G. Milewski, D. Engström, and J. Bengtsson, *Appl. Opt.* **46**, 95 (2007).
13. D. Palima and V. R. Daria, *Appl. Opt.* **46**, 4197 (2007).
14. S. Y. Wu, J. Liang, and M. F. Becker, *Proc. SPIE* **8254**, 82540C (2012).
15. D. W. K. Wong and G. Chen, *Appl. Opt.* **47**, 602 (2008).
16. H. Zhang, J. Xie, and J. Liu, *Appl. Opt.* **48**, 5834 (2009).
17. P. A. Blanche, A. Bablumian, R. Voorakaranam, C. Christenson, W. Lin, and T. Gu, *Nature* **468**, 80 (2010).
18. B. Max and E. Wolf, *Principles of Optics* (Pergamon, 1980).
19. http://en.wikipedia.org/wiki/Peak_signal-to-noise_ratio